Supporting Information

Heat Generation in Single Magnetic Nanoparticles under Near Infrared Irradiation

Héctor Rodríguez-Rodríguez,[1,2] Gorka Salas,[1,3,*] and J. Ricardo Arias-Gonzalez[4,*]

[1]Instituto Madrileño de Estudios Avanzados en Nanociencia (IMDEA-Nanoscience), 28049 Cantoblanco, Madrid, Spain

[2]Departamento de Química-Física Aplicada, Universidad Autónoma de Madrid, 28049 Cantoblanco, Madrid, Spain

[3]CNB-CSIC-IMDEA Nanociencia Associated Unit "Unidad de Nanobiotecnología", 28049 Cantoblanco, Madrid, Spain

[4]Centro de Tecnologías Físicas, Universitat Politècnica de València, Camino de Vera s/n, 46022 Valencia, Spain

*J.R. A.-G. ricardo.ariasgonzalez@upv.es, ricardo.ariasgonzalez@gmail.com,

G.S. gorka.salas@imdea.org

Contents

Experimental section

Synthesis and encapsulation of the magnetic nanostructures

Magnetite (Fe_3O_4) NPs coated by silica (SiO_2) were prepared as reported in our previous work.[1] The sample characterization is shown in Fig. S1.

Optical characterization

Optical extinction was measured with a Cary 50 spectrophotometer from Varian. Luminescence in the optical trap was tested using a monochromator (Fluoromax 4, Horiba) and a photomultiplier tube (R928P, Hamamatsu).

Optical trapping experiments

The main experiments were carried out in a miniaturized single-beam optical tweezers with force calibrated by the photon linear momentum conservation method.[2] The laser beam (wavelength, $\lambda = 808$ nm) was focused through a microscope objective (UPLASAPO 60X, water immersion, NA 1.2; Olympus) inside a microfluidics chamber (180 μm-thick) in under-filling conditions thus giving rise to a weakly focused Gaussian beam (numerical aperture of the beams, $NA_b \approx 0.5$). According to the paraxial Helmholtz approximation for a weakly focused Gaussian beam, the estimated beam waist was near experimental validations, $2W_0 \approx 10^3$ nm, for setups with this optical design.[1] The maximum measured power at the trap was $P_{trap} \approx 130$ mW. The output beam was collected by means of an identical objective lens in order to monitor force measurements. Stokes' law assays were performed by moving the microfluidic chamber at velocities $|v_{drag}| < 100$ μm·s^{-1}, with simultaneous recording of the friction force, F_{drag}. The drag coefficient was obtained from linear fits to these experimental data, $\gamma = F_{drag}/v_{drag}$. Control experiments were performed with polystyrene calibration beads (Polybead Polyscience, 1 μm-diameter) using a counter-propagating double-beam trap. Room temperature was measured with a thermocouple in the vicinity of the microfluidics chamber.

Optical trapping stiffness characterization

Trap stiffnesses transversal and axial to the beam's propagating direction were measured and calculated as detailed in our previous work.[1] Stiffness measurements confirmed good agreement with the theory.

Nanostructure sample characterization

We prepared nanoparticles (NPs), both iron oxide NPs (IONPs) and silica-coated iron oxide (IONP@SiO_2) nanostructures, and performed rigorous optical trapping experiments to demonstrate all-optical confinement of the IONP@SiO_2 nanostructures in a weakly focused beam, as detailed in a previous work.[1] Here, we have used the same sample for coherence in the experimental procedure. In Fig. S1, we show again the transmission electron microscopy (TEM) characterization to provide a self-contained information.

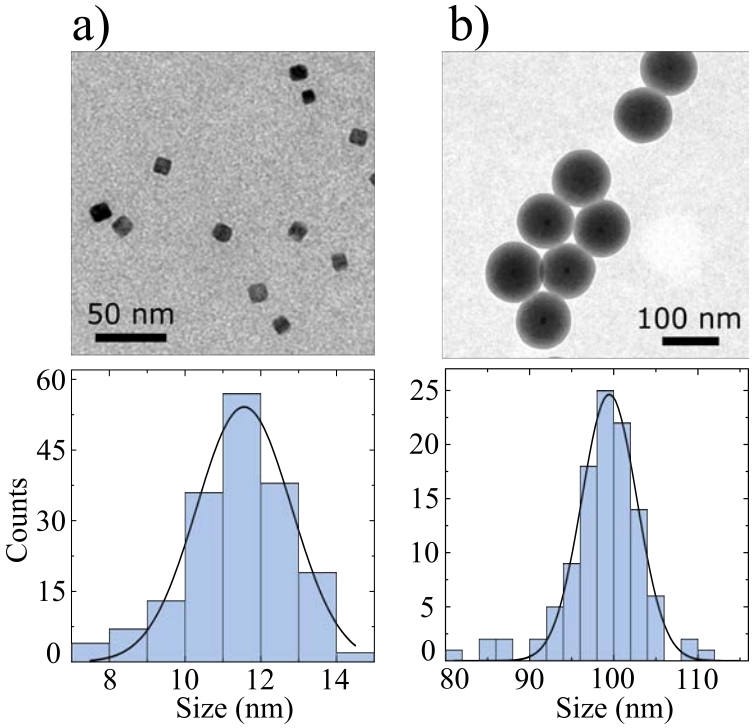

Figure S1. Top panels: TEM images of (a) IONPs and (b) IONP@SiO_2 nanostructures. Bottom panels, respective size histograms. Black curves are Gaussian fits. Mean diameter ± standard deviation values of 11 ± 1 and 99 ± 3 nm, for IONP cores and IONP@SiO_2 nanostructures, respectively, were determined through manual analysis of ensembles of over 300 particles in randomly selected areas of the transmission electron micrographs.

Luminescence of optically trapped silica-coated magnetic nanostructures

After optical excitation, an IONP@SiO_2 crystallite can release the absorbed energy both radiatively or non-radiatively. Broadband visible photoluminescence in magnetite nanocrystals has been reported under excitation at 407 nm.[3] In our experimental conditions, two-photon absorption processes may take place if the absorption cross section of the trapped NP is sufficiently large.[4-5] To investigate the occurrence of luminescent decay of our IONP@SiO_2 nanostructure, we flowed them into the microfluidics chamber at concentrations hundreds of times higher than those used for the main experiments (see section 3.3. in the main text). These conditions favor the trapping of multiple NPs in short times. Then, we registered the emission from the trap at 660 nm using a photomultiplier tube.

We collected the feasible emission light through the trapping objective and filtered it by means of a double-grating Czerny-Turner monochromator at 660 nm. We chose this wavelength to maximize the light transmission through the available optical elements. Despite the expected luminescent peak is centered at around 550 nm,[3] it is sufficiently broad and holds a significant intensity at 660 nm. The emission was analyzed with a photomultiplier tube (R928P, Hamamatsu). As shown in Fig. S2, no appreciable peak or intensity rise is found after the laser was switched on.

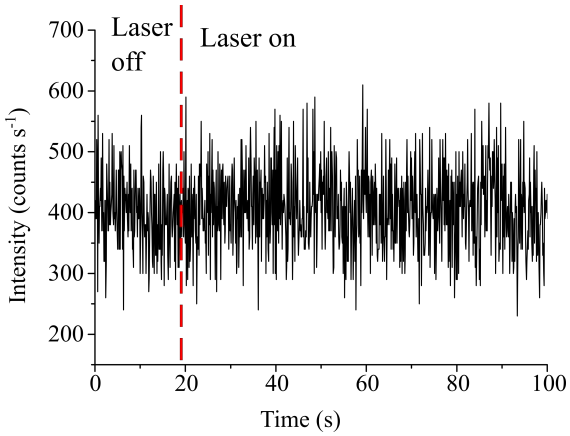

Figure S2. Optical trap intensity output at 660 nm as a function of the time. Red dashed line marks the instant when the trapping laser was switched on.

Since these experiments yielded negative results, we conclude that our sample presents negligible photoluminescence, both under one- and two-photon laser absorption, likely due to the presence of defects in the crystalline lattice.

Behavior of a single nanostructure in the optical trap

Single IONP@SiO_2 nanostructures exhibited stationary behavior in the laser beam focal region, which optically confines them. The resulting trap can be considered a Hookean potential well within the spatial region stochastically explored by the nanostructure. This is demonstrated by the excellent fitting of the measured position fluctuations to the power spectral density (PSD) functional behavior of an overdamped particle in a harmonic field, Fig. S3 (a).

The corner frequency, $f_c = \kappa/2\pi\gamma$, increases with the optical power majorly because the optical trap becomes tighter (trap stiffness, κ, increases), Fig. S3 (b). Due to optical heating from the IONP@SiO_2 nanostructure, as analyzed in the main text, viscosity decreases with optical power in the trap, making friction coefficient, γ, also decrease. As a result, the corner frequency also increases due heating effects.

The temperature dependence of the water viscosity (in Pa·s) can be approached by the next expression:[6]

$$\log\left(\eta_{H_2O}\right) = \frac{1.3272\times(293.15 - T) - 0.001053\times(T - 293.15)^2}{T - 168.15} - 2.999 \qquad \text{(S1)}$$

where 'log' is the logarithm with base 10 and T the absolute temperature, such that $T > 293.15$ K.

The microfluidics chamber was displaced with respect to the optical trap during Stokes' law measurements (see Methods in the main text). For powers in the trap at or below $P_{trap} = 60$ mW, velocities had to be limited above because drag forces made the specimen escape from the trap. In this regard, it interesting to note that optical trapping was achieved at powers as low as 30 mW but reliable Stokes' law measurements were not possible in these conditions.

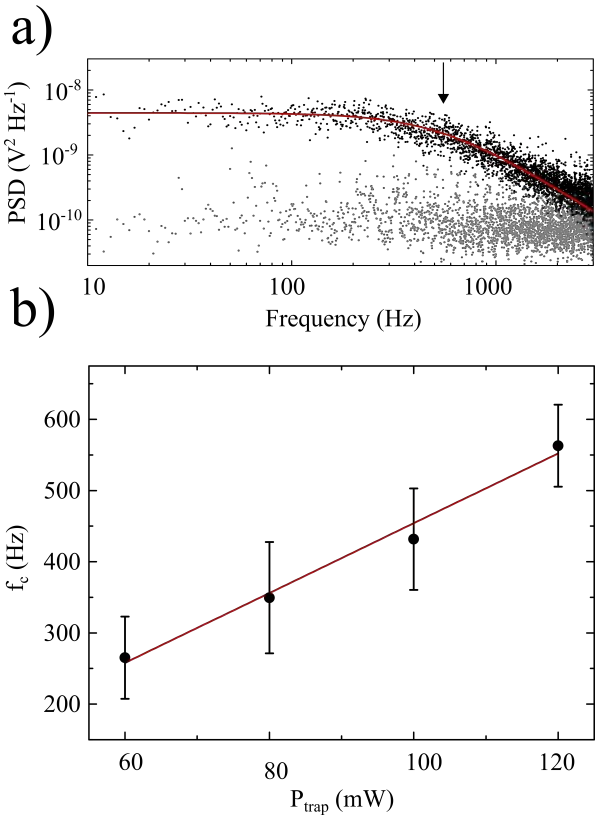

Figure S3. Thermal analysis of an individually trapped IONP@SiO_2 nanostructure. (a) Black dots, power spectrum density of transversal position fluctuations of a single IONP@SiO2 trapped at a power $P_{trap} = 120$ mW. Grey dots, power spectrum density of the empty trap under the same conditions. The red curve is a Lorentzian fit with corner frequency $f_c = 535 \pm 5$ Hz, marked by a vertical black arrow. (b) Dependence of the measured f_c with P_{trap}. Black dots are mean ± SD over three representative nanostructures. The red line is a linear fit to the experimental data.

Heat equation for silica-coated magnetic nanostructures

Energy from light impinging an IONP@SiO_2 nanostructure is dissipated as heat, as discussed above, and conducted thermally through the silica interface to the water surrounding the nanostructure, where it is spread in radial directions, r. The heat generation rate in stationary conditions equals the absorbed power ($\dot{q} = P_{abs}$). The temperature increase around the magnetic core is estimated by solving Fourier's law for heat conduction in a spherical symmetry:

$$\int_{T}^{T_0} dT' = -\frac{P_{abs}}{4\pi C}\int_{r}^{\infty} r'^{-2} dr' , \qquad \text{(S2)}$$

where T is the absolute temperature and C is the thermal conductivity of the medium surrounding the heat source. In our system, Fig. S4, after applying $T(r \to \infty) = T_0$ (room temperature) as a boundary condition and considering that only the magnetic core absorbs light, we find:

$$\Delta T(r) = T(r) - T_0 = \begin{cases} \dfrac{P_{abs}}{4\pi C_w r}\ , & r \geq a \quad \text{(S3a)} \\ \dfrac{P_{abs}}{4\pi C_{sa} r} + \dfrac{P_{abs}}{4\pi a}\left(\dfrac{1}{C_w} - \dfrac{1}{C_{sa}}\right), & a_c \leq r \leq a \quad \text{(S3b)} \\ \dfrac{P_{abs}}{8\pi C_c}\dfrac{a_c^2 - r^2}{a_c^3} + \dfrac{P_{abs}}{4\pi}\left[\dfrac{1}{C_{sa} a_c} + \dfrac{1}{a}\left(\dfrac{1}{C_w} - \dfrac{1}{C_{sa}}\right)\right], & r \leq a_c \quad \text{(S3c)} \end{cases}$$

where a_c and a are the radius of the IONP core and the IONP@SiO_2 nanostructure, respectively; C_{sa}, C_w and C_c are the thermal conductivities of silica, water and the magnetic core, respectively; and P_{abs} is the light power absorbed by the core. Equation (S3c) confirms that the temperature rise remains finite within the absorbing core.

The temperature rise is linear with the absorbed power but not necessarily with the power in the trap. For motionless nanostructures (e.g. affixed on a solid surface), the absorbed power is constant with the spatial coordinates. In our situation, the nanostructure presents a Brownian motion due to the water molecule collisions and then the absorbed power depends on the position within the focal region, as studied below.

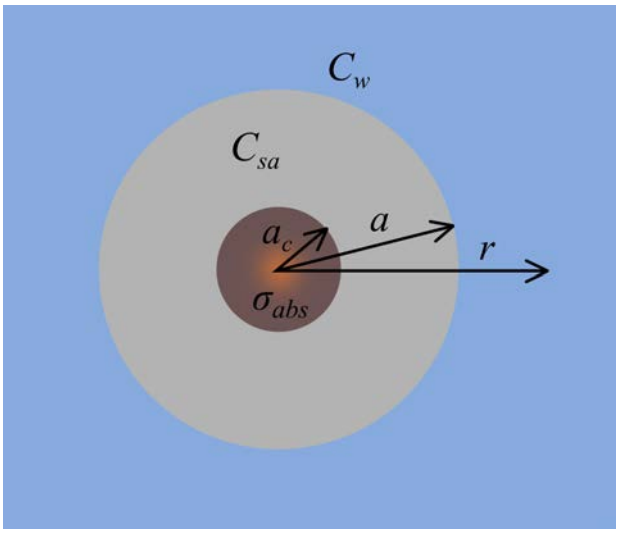

Figure S4. Schematic of the IONP@SiO2 nanostructure (not to scale) consisting of a magnetic core (brown) and a SiO_2 shell (grey) in water (blue). a_c and a are the radius of the magnetic core and silica shell, respectively; C_{sa} and C_w are the thermal conductivity of silica and water, respectively and σ_{abs}, the absorption cross section of the whole nanostructure. r is the radial distance from the center of the magnetic core.

Power absorbed by an optically trapped nanostructure

The use of a Gaussian beam theory to account for the focusing of the laser beam is accurate for weak focusing (numerical aperture of the beams, $NA_b \approx 0.5$, see Methods), as we previously demonstrated.[1] The laser beam intensity, $I(\rho, z)$, of a weakly focused laser beam is:[7]

$$I(\rho, z) = I_{inc}\left(\frac{W_0}{W(z)}\right)^2 \exp\left(-\frac{2\rho^2}{W^2(z)}\right) \quad \text{(S4)}$$

where ρ is the polar radial coordinate in planes perpendicular to the beam's propagating direction and z the axial coordinate (i.e., along the optical axis) with origin at the focal region center (cylindrical symmetry), $W(z) = W_0\sqrt{1 + (z/z_0)^2}$ and $W_0 = \sqrt{\lambda z_0/n\pi}$ are the beam width and waist radius, respectively, z_0 the Rayleigh range and I_{inc} the intensity at the center of the focal region ($\rho = z = 0$). To deduce values for W_0 and z_0 from the measured beam's numerical aperture ($\mathrm{NA}_b = n \sin\theta_0$; n, the refractive index of water and θ_0, the beam's divergence angle), we use $W_0 = \lambda/(\pi \mathrm{NA}_b)$ and $z_0 = \lambda n/(\pi(\mathrm{NA}_b)^2)$, see Methods and Ref. 1. The power in the trap, P_{trap}, is calculated as a surface integral at planes transversal to the Gaussian beam propagating direction:

$$P_{trap} = \int I(\rho, z) dS = I_{inc} \frac{1}{2} \pi W_0^2, \tag{S5}$$

This result does not depend on the axial coordinate z.[7]

Since the particle is smaller than the focal region, the power that it absorbs is position-dependent. The position probability density (in inverse volume units), $\mathrm{Prob}[\rho, z]$, describes the spatial fluctuations of the particle; having in mind that the system is ergodic and that the dynamics of the particle is stationary, the ensemble can be modeled by the canonical distribution using only the elastic energies of the particle in the trap. In addition, for displacements near the equilibrium position, we can use a Hooke's law. Then:

$$\mathrm{Prob}[\rho, z] = \frac{\kappa_\rho \sqrt{\kappa_z}}{(2\pi k_B T)^{3/2}} \exp\left(-\frac{\kappa_\rho \rho^2 + \kappa_z z^2}{2 k_B T}\right), \tag{S6}$$

being κ_ρ and κ_z the transversal and axial trap stiffnesses, respectively, and $k_B T$, the thermal energy (k_B, the Boltzmann constant). For a stationary dynamics, we used the average absorbed power instead, which we evaluate by integrating the local intensity received by the particle as it explores the focal volume:

$$P_{abs} = \sigma_{abs} \iint I(\rho, z)\, \mathrm{Prob}[\rho, z]\, dS\, dz\,. \tag{S7}$$

The volume element consists of the transversal surface element, dS, and the line element along the optical axis, dz. The absorbed power, which is a spatial average, can be considered a time-average magnitude since the system is stationary, and an ensemble-average magnitude over trapping experiments similarly prepared due to ergodicity. We analyze Eq. (S7) in three different regimes:

(1) Weak confinement: the particle motion is not restricted within the focal volume. The integral in Eq. (S7) without approximation reads:

$$P_{abs} = P_{trap} \frac{\kappa_\rho \sqrt{2\kappa_z}\sigma_{abs}}{\sqrt{\pi^3 k_B T}} \int_{-\infty}^{+\infty} dz \frac{\exp\left(-\frac{\kappa_z z^2}{2 k_B T}\right)}{\kappa_\rho W_0^2 [1 + (z/z_0)^2] + 4 k_B T}, \tag{S8}$$

(2) Moderate confinement: $z \ll z_0$. The particle fluctuates near the focal region center and, as a result, the absorbed power reduces to:

$$P_{abs} \approx \frac{2}{\pi} \frac{\kappa_\rho \sigma_{abs}}{\kappa_\rho W_0^2 + 4k_B T} P_{trap} \,. \tag{S9}$$

(3) Strong confinement: $z \ll z_0$ and $\sqrt{\langle \rho^2 \rangle} \ll W_0$ (where $\langle \rho^2 \rangle$ is the mean square displacement of the particle in the transversal plane located at $z = 0$). By using the Equipartition Theorem, $\kappa_\rho \langle \rho^2 \rangle / 2 = 2\, k_B T/2$, the second condition implies that $\kappa_\rho W_0^2 \gg 2k_B T$, that is, that the thermal energy level is very low compared to the trapping potential energy, and therefore

$$P_{abs} \approx \sigma_{abs} I_{inc} = \frac{\sigma_{abs}}{\frac{1}{2}\pi W_0^2} P_{trap} \,, \tag{S10}$$

where we have used Eq. (S5). Certainly, for a tightly-trapped particle, $\mathrm{Prob}[\rho, z] = \delta(\rho)\delta(z)/2\pi\rho$ (Dirac delta distribution in cylindrical coordinates) and Eq. (S7) reduces to Eq. (S10). This expression is linear in the trap power and it is a good approximation for near-micron-sized particles or high-refractive index NPs.

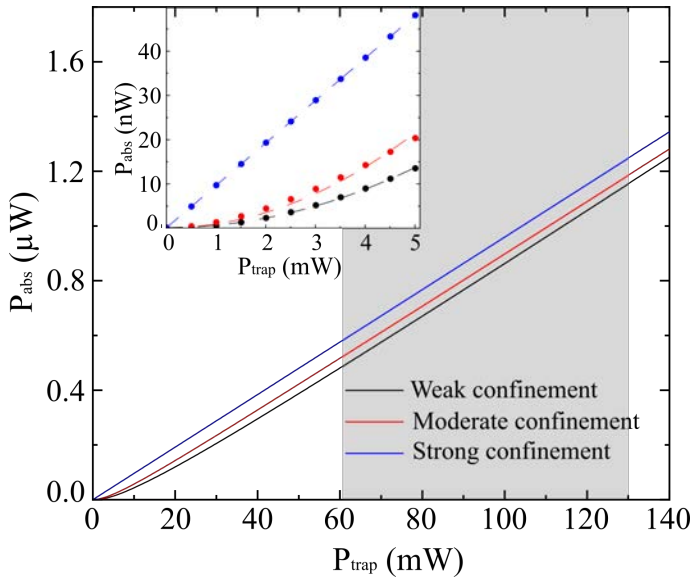

Figure S5. Power absorbed by a single magnetic nanostructure in an optical trap. Dependence of the absorbed power on the trapping power in the case of weak (Eq. (S8), black line), moderate (Eq. (S9), red line), and strong (Eq. (S10), blue line) confinement. The grey-shaded area represents the accessible trapping powers in our experimental conditions: below $P_{trap} < 60$ mW Stokes' test on single IONP@SiO_2 could not be performed, while P_{trap} at the diode laser limiting current was ~130 mW). Inset, detail at $P_{trap} < 5$ mW. Dots are calculations according to Eq. (S8), Eq. (S9) and Eq. (S10) while dashed curves are the best linear (strong confinement) and quadratic (moderate and weak confinement) fittings.

By combining Eq. (2a) and Eq. (2b) in the main text with Eq. (S7), we find that Eq. (S8) is a valid approximation for our experimental configuration, being Eq. (S10) limited (Fig. S5). The Stokes' test can be performed at a minimum power of $P_{trap} = 60$ mW without losing the trapped nanoparticle as a result of the viscous drag and the maximum

power allowed by the two laser diodes is $P_{trap} = 130$ mW. Within these limits, the nanostructure absorbs power from the laser beam following a linear trend. This fact indicates that, under our experimental conditions, optical power absorption is dominated by the trap irradiance. However, the effect of the motion of the nanostructure away from the laser focus center is patent at $P_{trap} < 5$ mW.

The increase in temperature around an IONP@SiO_2 nanostructure is represented in Fig. S6 at four different laser powers. We used $C_w = 0.60$ W·K^{-1}·m^{-1} and $C_{sa} = 0.95$ W·K^{-1}·m^{-1}, which is a reasonable value for porous silica.[6, 8]

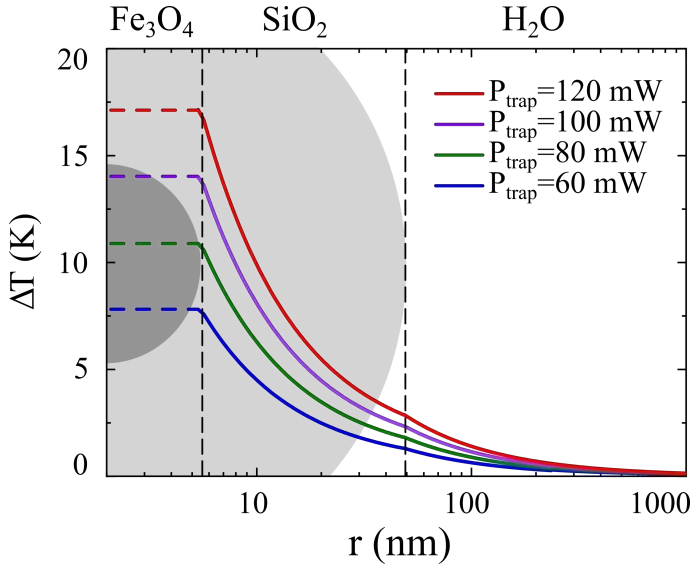

Figure S6. Theoretical temperature increment profile around a single magnetic nanostructure. The curves show results from Eq. (S3) combined with Eq. (S8) at four different trapping powers and in water. Vertical dashed lines mark core/shell and shell/water interface limits. The temperature increment has not been defined inside the magnetic core.

Relation between the power in the trap and the power absorbed by a nanostructure

To understand the non-linear relation between the power in the trap and the power absorbed by the nanostructure, we study the axial and transversal stiffnesses for a NP trapped in a weakly focused beam, as approximated considering $z \ll z_0$, $\rho \ll W_0$ (see Ref. 1 and the previous section in this document) in SI units:

$$\kappa_\rho = \Re e\{\alpha\}\frac{I_0}{W_0^2} \quad , \tag{S11}$$

$$\kappa_z = \Re e\{\alpha\}\frac{1}{2}\frac{I_0}{z_0^2} \quad , \tag{S12}$$

where α is the complex polarizability of the IONP@SiO_2 nanostructure, $I_0 = |E_0|^2$ the square modulus of the electric field, W_0 the waist radius and z_0 the Rayleigh range.[7] Following Eq. (S5),[7] the power in the trap is:

$$P_{trap} = I_{inc}\frac{1}{2}\pi W_0^2 = \frac{cn}{16} I_0 W_0^2 (4\pi\varepsilon_0)\,, \tag{S13}$$

where I_{inc} has been expressed in terms of fundamental parameters in SI units, namely, $I_{inc} = I_0 cn\varepsilon_0/2$, with c the vacuum light speed, ε_0 the vacuum permittivity and n the refractive index of the surrounding medium.[1]

Then, it is possible to express the transversal and axial spring constants as linear functions of the power in the trap:

$$\kappa_\rho = \frac{4\Re e\{\alpha\}}{cn\varepsilon_0\pi W_0^4} P_{trap}\,, \tag{S14}$$

$$\kappa_z = \frac{2\Re e\{\alpha\}}{cn\varepsilon_0\pi W_0^2 z_0^2} P_{trap}\,. \tag{S15}$$

Indeed, $\kappa_\rho = \xi P_{trap}$, with $\xi = 4\Re e\{\alpha\}/cn\varepsilon_0\pi W_0^4$, and $\kappa_z = \zeta P_{trap}$, with $\zeta = 2\Re e\{\alpha\}/cn\varepsilon_0\pi W_0^2 z_0^2$.

A representation of the theoretical relationship between P_{abs} and P_{trap} is shown in Fig. S5, where we have used the numerical integration of Eq. (S8) together with Eqs. (S9) and (S10). In the strong confinement regime, Eq. (S10), $B \equiv \Delta T(r = R)/P_{trap}$ is a constant. In the weak and moderate confinement regimes (small particle in a weakly focused beam, Eqs. (S8) and (S9), respectively), there is also a contribution from the trapping stiffnesses, which increase with P_{trap}, as approached by Eqs. (S14) and (S15). Indeed, by expressing, $\kappa_\rho = \xi P_{trap}$ (with ξ, a real, positive constant), in Eq. (S9), we obtain the next approximation for the moderate confinement regime:

$$P_{abs} \approx \frac{2}{\pi}\frac{\xi\sigma_{abs}}{\xi W_0^2 P_{trap} + 4k_B T} P_{trap}^2\,, \tag{S16}$$

which squares with the power in the trap in the limit of low laser power ($P_{trap} < 20$ mW in our experimental conditions). However, as observed in Fig. S5, it follows a linear trend within the range of accessible trapping powers in our assays and therefore, we can apply Eq. (4) in the main text to our data.

Within the moderate confinement regime, the functional relationship between B and P_{trap} is (see Eq. (S16)):

$$B \equiv \frac{\Delta \mathrm{T}}{P_{trap}} \propto \frac{\xi\sigma_{abs}}{\xi W_0^2 P_{trap} + 4k_B T} P_{trap} = \frac{cP_{trap}}{dP_{trap} + f}\,, \tag{S17}$$

where $c, d, f > 0$ are parameters. For our setup and sample particle conditions, it happens that $c \ll f \ll d$ and therefore, B can be satisfactorily approximated by a constant within the applied laser power range ($P_{trap} \to \infty \Rightarrow B \sim c/d$). For low power in the trap, however, $P_{trap} \to 0 \Rightarrow B \sim cP_{trap}/f$; the heat coefficient becomes a linear function of the power in the trap, $B(P_{trap}) = b \times P_{trap}$, and the temperature rise a quadratic function of the power in the trap, $\Delta \mathrm{T} = b \times P_{trap}^2$.

Hydrodynamic diameter and laser heating factor of optically trapped nanostructures: Raw data

	d_{hydro} (nm)	SE	B (K W^{-1})	SE
1-NP	80.3	4.2	27.9	12.1
	96.9	5.6	21.6	14.1
	101.4	6.1	28.5	13.0
	105.3	5.8	18.3	24.8
	106.5	5.1	17.8	23.0
	113.1	3.2	28.4	13.4
	113.6	8.8	13.6	15.0
	114.4	5.1	25.5	20.4
	115.1	5.6	23.3	11.7
	115.5	4.4	20.9	18.3
	121.2	3.1	15.4	11.6
	113.0	3.0	34.0	7.0
Multi-NP	129.1	8.1	204.7	40.3
	129.8	5.2	35.8	18.5
	131.4	13.2	58.8	48.7
	133.1	5.2	144.4	22.5
	133.2	5.2	144.5	22.6
	135.3	4.9	235.5	23.0
	135.6	5.6	88.7	20.9
	136.1	7.7	68.4	27.5
	136.6	6.0	98.9	23.8
	138.9	5.4	147.8	22.0
	139.0	8.1	52.8	28.5
	140.6	3.6	112.9	13.8
	141.7	5.0	40.5	16.4
	142.7	4.1	119.6	15.4
	143.4	4.5	72.4	16.5
	144.7	4.9	97.5	17.8

	d_{hydro} (nm)	SE	B (K W^{-1})	SE
Multi-NP	146.0	5.7	134.0	22.2
	146.5	9.1	79.4	33.0
	146.7	7.0	79.2	24.0
	147.7	6.1	133.0	23.1
	148.8	5.5	78.9	18.8
	158.6	7.0	128.7	24.5
	159.8	3.5	46.4	10.3
	161.2	6.0	98.1	19.0
	162.9	6.6	268.7	26.8
	163.9	10.7	210.4	40.2
	167.2	4.0	82.6	11.9
	167.2	11.4	279.2	45.2
	167.7	4.7	110.2	15.3
	167.7	7.5	228.2	28.3
	168.1	16.0	224.2	59.8
	168.2	3.8	77.7	11.1
	170.6	10.5	116.1	34.2
	170.8	12.5	271.8	48.5
	171.4	5.8	225.7	21.3
	175.8	10.3	180.4	33.6
	177.4	6.8	56.8	20.5
	180.2	11.2	188.4	37.2
	180.4	9.7	270.7	35.9
	184.2	8.2	82.7	22.3
	184.2	3.2	198.7	11.0
	185.6	15.8	173.0	48.8
	185.9	12.5	275.8	44.5
	187.6	13.0	179.5	39.7

	d_{hydro} (nm)	SE	B (K W^{-1})	SE
Multi-NP	192.1	9.2	285.0	32.2
	193.7	10.3	256.1	34.4
	195.7	11.6	413.5	45.3
	196.6	8.2	357.4	30.4
	202.5	8.5	349.3	30.4
	205.5	10.9	149.7	29.1
	209.8	11.9	338.5	40.7
	210.6	7.1	344.4	24.1
	220.0	15.1	332.6	48.9
	220.1	18.2	468.5	68.4
	229.8	15.7	293.0	45.3
	233.3	7.1	295.5	20.5
	240.1	15.9	514.7	56.1
	244.7	29.4	409.3	91.4
	246.1	22.1	477.1	73.3
	246.7	16.0	450.6	52.6
	250.0	18.3	488.1	62.1
	258.8	23.4	459.1	72.7
	258.9	12.4	522.4	40.9
	285.2	15.3	529.4	45.8
	286.0	22.2	436.5	60.4
PS-Beads	1054.8	18.5	2.1	5.8
	1064.0	7.2	2.0	2.1
	1012.4	5.6	4.1	1.6
	1047.1	5.2	5.3	1.6
	1074.1	9.6	5.3	2.9
	1021.3	7.4	4.0	2.3

Temperature rise due to water absorption

For small NPs, it is a good approximation to consider the temperature rise within the focal region due to water absorption as an independent effect, which adds to the temperature rise produced by the NP. The heating coefficient due to plain light absorption by water within the focal region, $B_w^{in} \equiv \Delta T_w / P_{trap}$, is:[9-10]

$$B_w^{in}(r) = B_w^{out}(W_0)\left[1 + \frac{1}{2\ln(D/2W_0)}\left(1 - \frac{r^2}{W_0^2}\right)\right], \quad 0 \le r \le W_0 \qquad \text{(S17)}$$

being 'ln' the natural logarithm and

$$B_w^{out}(r) = \frac{\alpha_w}{2\pi C_w} \ln\frac{D}{2r}, \qquad W_0 \le r \le D/2 \qquad \text{(S18)}$$

the heating coefficient outside the focal region, which is evaluated at the limiting surface, $B_w^{out}(r = W_0)$, in Eq. (S17). Parameters in our experiments are: $\alpha_w \approx 1.95$ m^{-1}, the absorption coefficient of water at $\lambda_{trap} = 808$ nm;[11] $D \approx 180$ μm, the distance between the walls of the microfluidic chamber and $W_0 \approx 0.5$ μm (Methods). Then, the laser-induced heating coefficients of water comply with $B_w^{in}, B_w^{out} < 3$ K·W^{-1} and the temperature rise inside or outside the focal region keeps $\Delta T_w < 0.3$ K at $P_{trap} = 100$ mW.

Supporting references

1. Rodríguez-Rodríguez, H.; de Lorenzo, S.; de la Cueva, L.; Salas, G.; Arias-Gonzalez, J. R. Optical Trapping of Single Nanostructures in a Weakly Focused Beam. Application to Magnetic Nanoparticles. *J. Phys. Chem. C* **2018**, *122*, 18094-18101.
2. Smith, S. B.; Cui, Y.; Bustamante, C. Optical-trap force transducer that operates by direct measurement of light momentum. *Methods Enzymol.* **2003**, *361*, 134-162.
3. Sadat, M. E.; Kaveh Baghbador, M.; Dunn, A. W.; Wagner, H. P.; Ewing, R. C.; Zhang, J.; Xu, H.; Pauletti, G. M.; Mast, D. B.; Shi, D. Photoluminescence and photothermal effect of Fe3O4 nanoparticles for medical imaging and therapy. *Appl. Phys. Lett.* **2014**, *105*, 091903-091903.
4. Hormeño, S.; Bastús, N. G.; Juárez, B. H.; Pietsch, A.; Weller, H.; Arias-Gonzalez, J. R. Plasmon-Exciton Interactions on Single Thermoresponsive Platforms Demonstrated by Optical Tweezers. *Nano Lett.* **2011**, *11*, 4742-4747.
5. Rodriguez-Rodriguez, H.; Acebron, M.; Juarez, B. H.; Arias-Gonzalez, J. R. Luminescence Dynamics of Silica-Encapsulated Quantum Dots During Optical Trapping. *J. Phys. Chem. C* **2017**, *121*, 10124-10130.
6. Weast, R. C. CRC Handbook of Chemistry and Physics. 53rd ed.; CRC Press: Boca Raton, Florida, **1973**.
7. Saleh, B. E. A.; Teich, M. C. Fundamentals of Photonics. 3 ed.; John Wiley & Sons: New York, **2007**.
8. Nield, D. A.; Bejan, A., Heat Transfer Through a Porous Medium. In Convection in Porous Media, Nield, D. A.; Bejan, A. Eds. Springer: New York, NY, **2013**; pp 31-46.
9. De Lorenzo, S.; Ribezzi-Crivellari, M.; Arias-Gonzalez, J. R.; Smith, S. B.; Ritort, F. A Temperature-Jump Optical Trap for Single-Molecule Manipulation. *Biophys. J.* **2015**, *108*, 2854-2864.
10. Mao, H.; Arias-Gonzalez, J. R.; Smith, S. B.; Tinoco, I.; Bustamante, C. Temperature control methods in a laser tweezers system. *Biophys. J.* **2005**, *89*, 1308-16.
11. Palmer, K. F.; Williams, D. Optical properties of water in the near infrared. *J. Opt. Soc. Am.* **1974**, *64*, 1107-1110.